arXiv:2009.06753v1 [cond-mat.supr-con] 14 Sep 2020

Effect of controlled point-like disorder induced by 2.5 MeV electron irradiation on nematic resistivity anisotropy of hole-doped (Ba,K)Fe_2As_2

M. A. Tanatar,[1,2] Erik I. Timmons,[1,2] M. Kończykowski,[3] O. Cavani,[3]
Kyuil Cho,[1] Yong Liu,[1] T. A. Lograsso,[1,4] and R. Prozorov[1,2]

[1] *Ames Laboratory, USDOE, Ames, Iowa 50011, USA*
[2] *Department of Physics and Astronomy, Iowa State University, Ames, Iowa 50011, USA**
[3] *Laboratoire des Solides Irradis, CEA/DRF/lRAMIS, Ecole Polytechnique, CNRS, Institut Polytechnique de Paris, F-91128 Palaiseau, France*
[4] *Department of Material Science and Engineering, Iowa State University, Ames, Iowa 50011, USA*

(Dated: February 20, 2024)

In-plane anisotropy of electrical resistivity was studied in samples of the hole-doped $Ba_{1-x}K_xFe_2As_2$ in the composition range $0.21 \leq x \leq 0.26$ where anisotropy changes sign. Low-temperature (∼20 K) irradiation with relativistic 2.5 MeV electrons was used to control the level of disorder and residual resistivity of the samples. Modification of the stress-detwinning technique enabled measurements of the same samples before and after irradiation, leading to conclusion of anisotropic character of predominantly inelastic scattering processes. Our main finding is that the resistivity anisotropy is of the same sign irrespective of residual resistivity, and remains the same in the orthorhombic C_2 phase above the re-entrant tetragonal transition. Unusual T-linear dependence of the anisotropy $\Delta\rho \equiv \rho_a(T) - \rho_b(T)$ is found in pristine samples with x =0.213 and x =0.219, without similar signatures in either $\rho_a(T)$ or $\rho_b(T)$. We show that this feature can be reproduced by a phenomenological model of R. M. Fernandes *et al.* Phys. Rev. Lett. **107**,217002 (2011). We speculate that onset of fluctuations of nematic order on approaching the instability towards the re-entrant tetragonal phase contributes to this unusual dependence.

I. INTRODUCTION

Studies of in-plane anisotropy of electrical resistivity in iron-based superconductors are performed on stress-detwinned samples [1, 2] creating preferential orientation of orhthorombic domains [3]. The resistivities for principal orthorhombic directions, a and b, $\rho_a(T)$ and $\rho_b(T)$, and their difference $\Delta\rho \equiv \rho_a - \rho_b$ referred to as anisotropy, reveal several unusual features. The resistivity of the parent $BaFe_2As_2$ is lower for the long $a-$axis, $\rho_a < \rho_b$, corresponding to the antiferromagnetic chains in the stripe magnetic structure. The anisotropy increases with electron doping [and suppression of the orthorhombic distortion $\delta = (a-b)/(a+b)$], taking maximum near optimal doping on electron-doped side [2]. The anisotropy changes sign on the hole-doped side [4], with $\rho_a > \rho_b$, see phase diagram, Fig. 1. The mechanism of this sign change in the electronic transport attracts notable interest, since contributions from both elastic scattering due to impurities/defects [5, 6] and inelastic scattering on magnetic excitations [7, 8] and phonons can be anisotropic.

The magnitude of the anisotropy strongly depends on sample residual resistivity, as found in the study on the annealed samples [9–11]. It was argued [8] that the sign change of the resistivity anisotropy can be caused by dramatic difference in the levels of disorder scattering on the electron-doped side in $Ba(Fe_{1-x}TM_x)_2$ (TM= Co, Ni, Rh, Ir [12, 13]) and the hole-doped side in $Ba_{1-x}K_xFe_2As_2$ [14–17], as summarized in the bottom panel of Fig. 1. Indeed, substitution in the electronically active Fe sites introduces high level of scattering, with residual resistivity extrapolating to 100 $\mu\Omega cm$ or so close to optimal doping. The K-substitution in $Ba_{1-x}K_xFe_2As_2$ proceeds in electronically inactive Ba site and the residual resistivities are typically close to 30 $\mu\Omega cm$. This difference may imply that the sign may be the same for all the phase diagram.

Another consideration regarding the origin of the sign change is related to approaching the composition range of the re-entrant tetragonal C_4 phase [15, 18, 19]. At ambient pressure for compositions $x <\sim 0.24$ the samples of $Ba_{1-x}K_xFe_2As_2$ undergo simultaneous structural (tetragonal to orthorhombic) and magnetic (paramagnetic to stripe antiferromagnetic) transition below T_{C2} (see phase diagram Fig. 1). For $x > 0.24$ a sequence of phase transitions is observed, with re-entrance of the tetragonal phase below T_{C4} with complicated antiferromagnetic structure [20]. This phase was not known at the time of resistivity anisotropy study [4].

We have recently succeeded controlling the residual resistivity of the iron-based superconductors using low-temperature electron irradiation with relativistic 2.5 MeV electrons [21–23] and achieving residual resistivity levels comparable to the electron-doped side, as shown in Fig. 1 with open dots for x =0.20 [21], solid red circles and magenta stars (x =0.213 and x=0.260, respectively, this study). Disorder introduced by irradiation does not change carrier density and enables disentangling effects of doping and of the substitutional disorder, which are intertwined in the electron-doped $Ba(Fe_{1-x}TM_x)_2$. We use this development to study electrical resistivity anisotropy

* tanatar@ameslab.gov

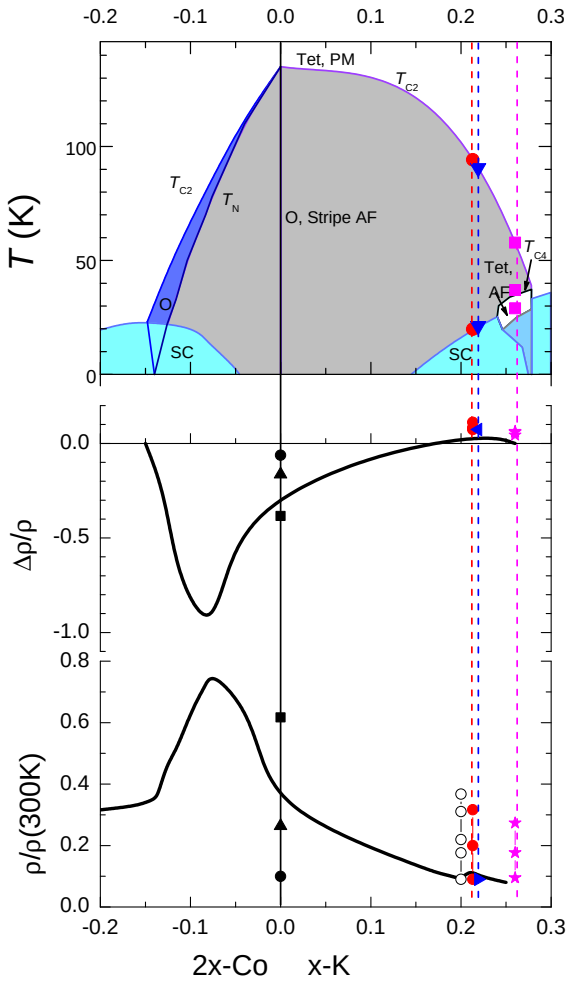


FIG. 1. (Color online) Top panel. Summary phase diagram of electron-, $Ba(Fe_{1-x}Co_x)_2As_2$, and hole-, $Ba_{1-x}K_xFe_2As_2$, doped iron based superconductors. Red, blue and magenta points are T_{C2}, T_c and T_{C4} of the pristine samples x =0.213, 0.219 and 0.260 respectively, used in this study. Middle panel shows composition dependence of the low-temperature resistivity anisotropy, $\Delta\rho/\rho$, where $\Delta\rho = \rho_a - \rho_b$. Black solid symbols in the middle and bottom panels show effect of residual resistivity on resistivity anisotropy at low temperatures in parent $BaFe_2As_2$, squares after [1], triangles after [11] and circles after [9]. Red, blue and magenta symbols are from this study. Bottom panel shows evolution of the resistivity ratio, $\rho(0)/\rho(300K)$ taken as a proxy of the residual resistivity. Open black circles are for the samples with x =0.20 subjected to electron irradiation [21], red and magenta symbols from the samples studied in this article, x =0.213 and x =0.260, in the sign reversal composition range. Blue is for the sample with x =0.219 studied only in the pristine state.

in the sign change composition range $0.21 \leq x \leq 0.26$. Two compositions selected for the irradiation study were x =0.213 and x =0.260. The first sample was on the orthorhombic, C_2, side of the composition boundary, the second one x =0.260 was in the re-entrant range. Our main finding is that the resistivity anisotropy is of the same sign irrespectively of residual resistivity, and remains the same in C_2 phase range above the re-entrant tetragonal transition.

II. EXPERIMENTAL

Single crystals of $Ba_{1-x}K_xFe_2As_2$ were grown as described in detail in Ref. 16. Large, above 5×5 mm^2 surface area crystals were cleaved on both sides to a thickness of typically 0.1 mm to minimize the variation of the K-content with thickness. The crystals from two different batches were used in this study with average compositions x_{av}=0.22 and 0.25, as determined from the electron-probe microanalysis with wavelength dispersive spectroscopy (WDS). The large slabs were cut using wire saw along the tetragonal [110] direction. Several cuts were made side by side to achieve the closest similarity of the sample properties. Multiple samples cut were mounted for four probe resistivity measurements. Contacts to the samples were tin-soldered [24, 25]. These contacts are strong enough to withstand multiple irradiation measurements [22] and the applications of stress [26]. Samples were pre-characterized by the electrical resistivity measurements, to ascertain reproducible properties. Despite identical WDS composition, samples revealed some variation in positions of features in $\rho(T)$ curves at the concomitant structural/magnetic transition T_{C2} and superconducting T_c. We account for this variation using polynomial fits of $T_{C2}(x)$ and $T_c(x)$ [27]. This was particularly important for samples from the batch with x_{av} =0.25, as these show some variation of the positions of T_{C2} and T_{C4} features in $\rho(T)$ even between the crystals cut from the same slab. Samples selected for irradiation in this study had x =0.213 and x =0.260 (±0.001). One more sample was used for control purposes, x =0.219, all compositions determined from the $T_{C2}(x)$ formula [27]. Use of $T_c(x)$ gave similar composition differences.

Due to high probability of formation of cracks during stress application, we prepared two samples of each composition. Only one sample of each composition eventually survived irradiation cycles without crack formation. The silver wires of potential contacts were used both for resistivity measurements and for stress application [1, 28]. We used a specially designed device enabling easy sample mounting/dismounting and controllable application of the tensile stress, shown in inset of the left panel in Fig. 3 below. Four-probe resistivity measurements were performed in a *Quantum Design* PPMS.

The low-temperature 2.5 MeV electron irradiation was performed at the SIRIUS Pelletron linear accelerator operated by the *Laboratoire des Solides Irradiés* (LSI) at the *Ecole Polytechnique* in Palaiseau, France [29]. The samples for resistivity measurements during and after electron irradiation were mounted on a thin mica plate in a hollow *Kyocera* chip, so that they could be moved between the irradiation chamber (in LSI) and the detwinning resistivity setup (in Ames laboratory) without

disturbing the contacts. The *Kyocera* chip was mounted inside the irradiation chamber and was cooled by a flow of liquid hydrogen to $T \approx 22$ K in order to remove excess heat produced by relativistic electrons upon collision. The flux of electrons amounted to about 2.7 μA of electric current through a 5 mm diameter diaphragm. This current was measured with the Faraday cup placed behind a hole in the sample stage, so that only transmitted electrons were counted. The irradiation rate was about 5×10^{-6} C/(cm^2·s) and large doses were accumulated over the course of several irradiation runs. The penetration depth of electrons in the hole-doped iron based superconductors is estimated as 1.3 mm [30], tin and silver used in the contacts have similar values, so that for samples of our dimensions the irradiation is homogeneous and there should be no shadow on the samples under the contacts. To stay on a safe side, though, the samples were positioned with electron beam incoming from the opposite to the contacts side of the samples. Throughout the manuscript we use "pristine" and "unirradiated" interchangeably to describe samples that were not exposed to electron irradiation.

Irradiation of a dose 1 C/cm^2 with 2.5 MeV results in about 0.07% of the defects per iron site [23]. The Frenkel pairs are created at about the same density in all sublattices. It is well known that in metals, self-diffusion of interstitials is much higher than that of vacancies, especially warming up above roughly 100 K or so and that they mostly diffuse out and disappear at various sinks, like extended defects (dislocations/disclinations) and surfaces [31]. A much slower to relax population of vacancies remain in the crystal in a quasi-equilibrium (metastable) state controlled by the highest temperature reached. Resistivity measurements *in situ* at 22 K during irradiation in $Ba_{1-x}K_xFe_2As_2$ with close composition x =0.20 [21] show linear increase with irradiation dose at a rate $\sim$ 50 $\mu\Omega$cm per 1 C/cm^2, decreasing to $\sim$ 30 $\mu\Omega$cm upon warming to room temperature due to defect annealing [21]. The dose of defects created by electron irradiation is negligible compared with electron and hole densities in a good metal like $Ba_{1-x}K_xFe_2As_2$, as verified experimentally by Hall effect measurements [21].

III. ELECTRICAL RESISTIVITY

In Fig. 2 we show evolution of the temperature-dependent resistivity of $Ba_{1-x}K_xFe_2As_2$, x =0.213, with electron irradiation. Measurements were done in stress-free conditions in the twinned state, with resistivity denoted as ρ_t. The evolution is consistent with our previous studies [21, 22], with suppression of the superconducting T_c (inset in left panel) and of the temperature of the structural/magnetic transition, T_{C2}, as seen in resistivity derivative plots (right panel). The increase of the resistivity is not constant in temperature and it is notably larger on $T \to 0$, revealing notable Matthiessen rule violation. The residual resistivity increases more than by a factor of 3, from $\sim$30 to $\sim$100 $\mu\Omega$cm.

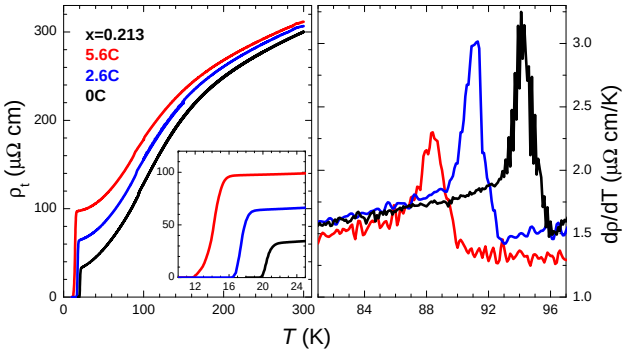


FIG. 2. (Color online) Temperature-dependent electrical resistivity of stress free twinned samples, $\rho_t(T)$, of $Ba_{1-x}K_xFe_2As_2$, x =0.213, with composition in the nematic anisotropy sign reversal range (left panel). Inset shows zoom of the superconducting transition. Black curves show data for sample before irradiation (0 C/cm^2), blue and red curves after irradiation with 2.6 C/cm^2 and 5.6 C/cm^2, respectively. Right panel shows temperature-dependent resistivity derivative for the data in the left panel revealing clear anomalies at the tetragonal to orthorhomic structural transition coinciding with the antiferromagnetic ordering, T_{C2}. Electron irradiation monotonically increases $\rho(0)$ from $\sim$30 to $\sim$100 $\mu\Omega$cm and suppresses both T_c and T_{C2} at approximately the same rate.

On application of tensile stress using hook horseshoe device [26] sample goes into the detwinned state with predominant orientation of domains with the orthorhombic a-axis along the stress direction. The resistivity increases with stress and saturates once detwinning action of stress is complete. The resistivity in this state, ρ_a, is shown in Fig. 3 with grey, cyan and magenta lines for 0, 2.6 and 5.6 C/cm^2 samples. The bottom curves show resistivity along b direction in the plane (black, blue and red curves for 0, 2.6 and 5.6 C/cm^2 respectively). Resistivity along b direction was determined assuming equal population of domains in the stress-free sample, $\rho_t = (\rho_a + \rho_b)/2$, and $\rho_b = 2\rho_t - \rho_a$.

The in-plane resistivity anisotropy, $\Delta\rho \equiv \rho_a - \rho_b$ is shown in the right panel of Fig. 3. The anisotropy sign remains the same for all irradiation doses with $\rho_a > \rho_b$. The anisotropy in pristine sample (black curve in the right panel of Fig. 3) reaches broad maximum at about $\sim$70 K and then decreases approximately linearly down to the superconducting transition. With 2.6 C/cm^2 irradiation, an increase of the residual resistivity from $\sim$ 30 to $\sim$60 $\mu\Omega$cm and shift of T_{C2} from 94 to 91 K, the maximum in $\Delta\rho(T)$ shifts to $\sim$60 K and some curvature starts to develop above T_c. The anisotropy above T_c notably increases compared to the pristine sample, from $\sim$2 to $\sim$7 $\mu\Omega$cm. Finally, with 5.6 C/cm^2 irradiation, increase of the residual resistivity to $\sim$100 $\mu\Omega$cm and T_{C2} suppression to 88 K, the maximum transforms into a plateau, starting somewhat below 60 K and continuing down to T_c. This $\Delta\rho(T)$ for 5.6 C/cm^2 irradiated

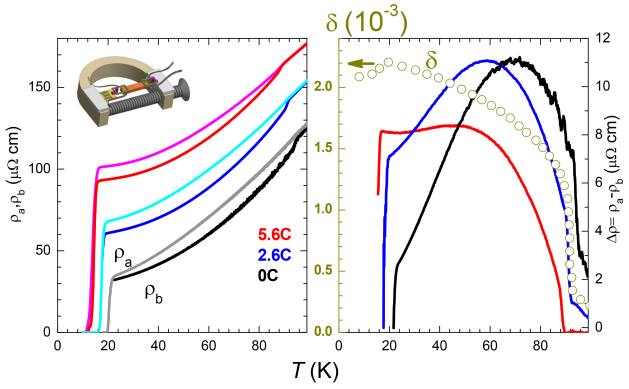


FIG. 3. (Color online) Temperature-dependent electrical resistivity of $Ba_{1-x}K_xFe_2As_2$ sample with x =0.213. Two sets of curves for each irradiation dose represent resistivity along $a-$, ρ_a (gray, cyan and magenta, top curves in the pair), and $b-$, ρ_b (black, blue and red, bottom curves in the pair), directions in the conducting plane. Right panel shows temperature-dependent in-plane resistivity anisotropy, $\Delta\rho \equiv \rho_a - \rho_b$, and its evolution with irradiation. Inset in the left panel shows hook device used for detwinning experiments with multiple mounting/dismounting cycles [26]. Sample is irradiated with 2.5 MeV electrons to introduce disorder in a controlled way between stress application runs. Open dark yeallow circles show temperature dependence of the nematic order parameter, $\delta = (a-b)/(a+b)$, left axis in the right panel, in sample with x =0.22 in thermal expansion measurements [18].

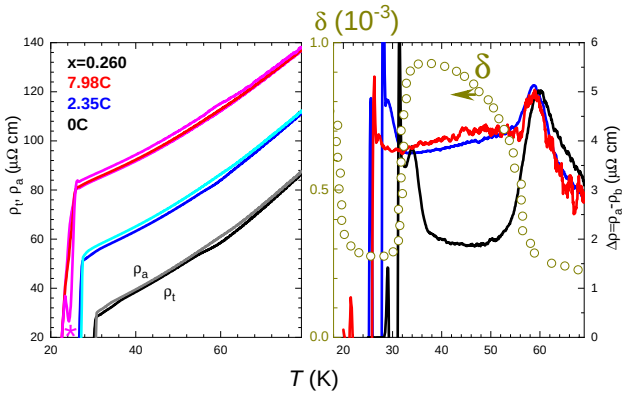


FIG. 4. (Color online) Temperature-dependent electrical resistivity of $Ba_{1-x}K_xFe_2As_2$ sample with x =0.260. Two sets of curves for each irradiation dose represent resistivity in stress free twinned state, $\rho_t(T)$, (black, blue and red for 0, 2.35 and 7.98 C/cm^2 respectively) and detwinned by application of tensile stress, $\rho_a(T)$ (gray, cyan and magenta for 0, 2.35 and 7.98 C/cm^2, respectively). Star marks partial cracking of the 7.98 C/cm^2 sample leading to a stress release. Right panel shows temperature-dependent in-plane resistivity anisotropy, $\Delta\rho \equiv \rho_a - \rho_b$, and its evolution with irradiation. For reference we show temperature evolution of nematic order parameter, $\delta = (a-b)/(a+b)$, (open dark yellow circles, left axis in the right panel), measured with thermal expansion technique in the sample with x =0.262 [18].

sample resembles temperature evolution of the nematic order parameter $\delta = (a-b)/(a+b)$, shown with dots (left scale in the right panel) from thermal expansion data of Böhmer *et al.* [18] for close x =0.22.

In the left panel of Fig. 4 we show evolution of the temperature dependent resistivity in $Ba_{1-x}K_xFe_2As_2$ sample with x =0.260. Measurements in stress-free conditions (black curve for pristine sample, blue and red for samples after irradiation with 2.35 and 7.98 C/cm^2, respectively) show monotonic increase of the resistivity. Note a feature at ∼30 K in the $\rho(T)$ curve for the sample with 7.98 C/cm^2 under stress (magenta line in Fig. 4) marked with the star. Here the sample partially cracked on cooling, with the stress release. Since this crack happened after the resistivity data were taken, we were able to determine the resistivity anisotropy as shown in the right panel 0f Fig. 4. However in the analysis below we use the data for 2.35 C/cm^2 sample. The features at T_{C2} (small increase on cooling below 60 K) and T_{C4} (small resistivity decrease below 35 K) are very sensitive to stress, which leads to sharp anomalies in the anisotropy plot in the right panel. With irradiation the T_{C4} is suppressed to at least below onset of the superconducting transition while the feature at T_{C2} is nearly unaffected.

Evolution of the in-plane resistivity anisotropy in the sample x =0.260 is quite remarkable. The stress-induced anisotropy in the tetragonal phases above T_{C2} and below T_{C4} is notably larger than in the orthorhombic phase. The overall magnitude of the anisotropy is about 2 times smaller than in x =0.213 sample. The temperature dependence of anisotropy has little resemblance to that in x =0.213, with anisotropy remaining nearly temperature-independent.

In Fig. 5 we show evolution of the resistivity and of the resistivity anisotropy at characteristic temperatures with irradiation dose. For sample with x =0.213 these temperatures were selected as T =60 K (in the vicinity of the maximum of anisotropy), at T =22 K (above onset of the superconducting transition) and in $T \to 0$ extrapolation. It is known that resistivity at a fixed temperature in irradiation chamber changes linearly with dose [21, 32], the Matthiessen rule is strongly violated in nearby x =0.20 composition. Interestingly, resistivity in $T \to 0$ extrapolation varies almost perfectly linearly with dose (black solid circles), but downward deviation from linear trend is found at 22 K and 60 K. Resistivity anisotropy at 60 K remains relatively constant. Resistivity anisotropy above T_c initially rises, then seems to saturate.

For sample with x =0.260 (bottom panel in Fig. 5) the resistivity increase for all temperatures has a tendency to downward deviation. One possibility is that this is an artefact of incorrect dose determination. Big doses are accumulated over several irradiation runs (during a period up to three years) and partial defect annealing can be happening over these long periods.

To check for systematics of the results, we measured one more pristine sample of $Ba_{1-x}K_xFe_2As_2$ from the

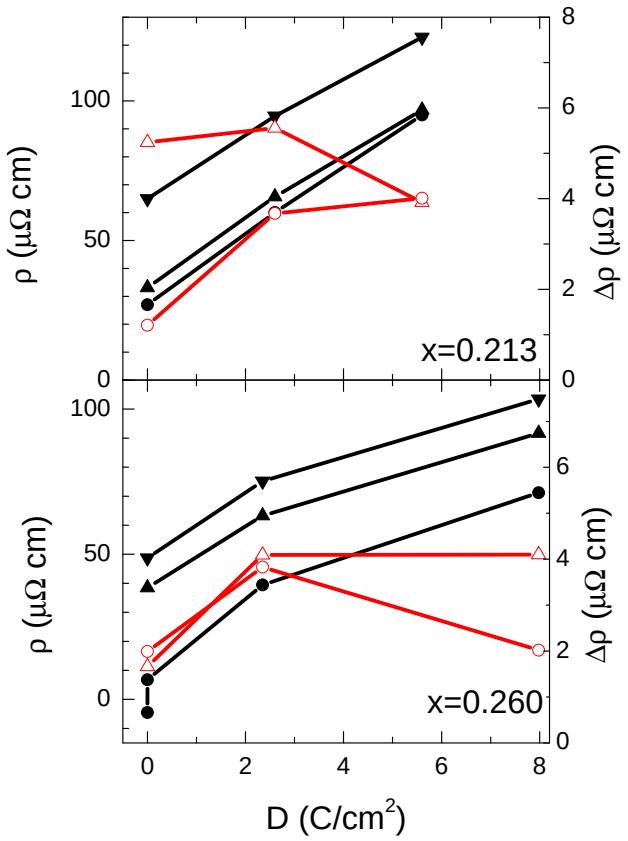


FIG. 5. (Color online) Irradiation dose dependence of resistivity (left axes, black symbols) and resistivity anisotropy (right axes, red symbols) in samples of $Ba_{1-x}K_xFe_2As_2$ with x =0.213 (top panel) and x =0.260 (bottom panel). In the top panel solid black down triangles and open red up-triangles are for T =60 K, at about maximum of anisotropy, solid up-triangles and open circles for T =22 K, just above T_c, and black solid circles in $T \to 0$ extrapolation. In the bottom panel solid black down triangles and open red up-triangles are for T =55 K, slightly below the T_{C4}, solid black up-triangles and open red circles are for T =38 K above T_{C4}, and solid black circles for T =0 extrapolation.

same batch as sample x =0.213, however, with somewhat different composition, x =0.219. The temperature-dependent electrical resistivity of the stress-detwinned sample with x =0.219 for measurements along principal in-plane directions, ρ_a and ρ_b, is shown in Fig. 6. The sample is characterised by somewhat lower T_{C2} compared to sample x =0.213 (inset in left panel of Fig. 6, 90.6 K vs 94 K) and higher T_c, 21.3 K vs 19.8 K. The resistivity curves show the same tendency as found in pristine sample with x =0.213, with two curves converging on cooling above T_c. In the right panel of Fig. 6 we show $\Delta\rho(T)$ for sample with x =0.219 (red line) in comparison with samples x =0.213 (black top curve) and x =0.260 (bottom blue curve). We can clearly see two trends with increasing x, the decrease of the maximum anisotropy and decrease of the slope of the linear portion of $\Delta\rho(T)$ (highlighted by lines serving as guides for eyes).

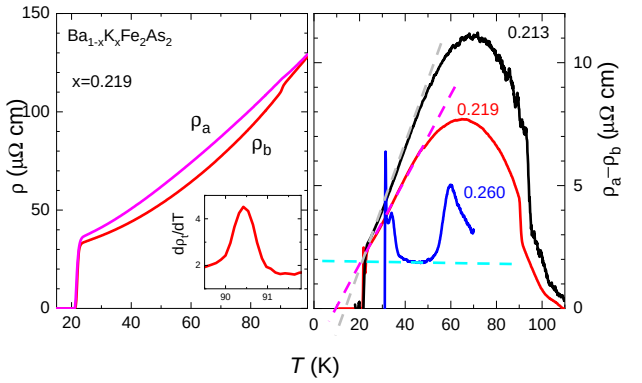


FIG. 6. (Color online) Temperature-dependent electrical resistivity of $Ba_{1-x}K_xFe_2As_2$ sample with x =0.219 for measurements along $a-$, ρ_a (top curve), and $b-$, ρ_b (bottom curve), directions in the conducting plane (left panel). Inset shows zoom of the structural/magnetic transition. Right panel shows temperature-dependent in-plane resistivity anisotropy, $\Delta\rho \equiv \rho_a - \rho_b$. For reference we show similar measurements in samples x =0.213 (black top curve) and x =0.260 (bottom blue curve). Dashed lines are guides for eyes.

IV. DISCUSSION

There are two main groups of theories explaining nematic resistivity anisotropy, see [33] for the review. The first group is relating the nematic anisotropy to the Drude term, n/m^*, reflecting anisotropy of the band structure. The other group of theories is relating $\Delta\rho$ to the anisotropy of scattering, both elastic and inelastic. In all theories the anisotropy should be proportional to the nematic order parameter, $\delta = (a-b)/(a+b)$, as found in scattering [19] and thermal expansion measurements [18] , the later shown in Fig. 3 and Fig. 4 for samples with x =0.22 and x =0.262, respectively. It is also possible to have a temperature dependent pre-factor Υ, coming, for example, from temperature dependent scattering in which case it should be proportional to ρ. The analysis of nematic resistivity anisotropy using this approximation, $\Delta\rho = \rho_t\delta$, was very successful in FeSe [34], giving quite good description of the data. We need to keep in mind though, that the situation in FeSe is simpler than in the hole doped $Ba_{1-x}K_xFe_2As_2$. Nematic order is not accompanied by the long range magnetic ordering in FeSe, and thus no Fermi surface folding effects are involved [35, 36]. On the contrary, the Fermi surface changes at the transition are important for the hole doped compositions studied here.

We start with analysis of the heavily irradiated samples, as shown in the left panel of Fig. 7. Here we compare directly $\Delta\rho(T)$ of the sample with x =0.213 irradiated with 5.6 C/cm^2 (black line) with $\delta(T)$ measured by Böhmer (dark yellow circles) and a product of resistivity in the twinned state $\rho_t(T)$ and $\delta(T)$ (dark yellow line). For reference we show $\Delta\rho(T)$ for 2.35 C/cm^2 ir-

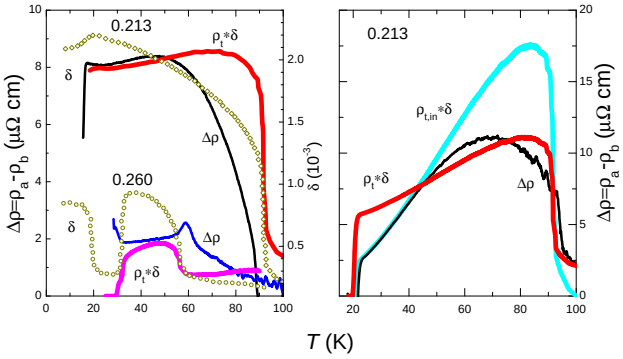


FIG. 7. (Color online) Left panel. Comparison of the in-plane resistivity anisotropy in samples of $Ba_{1-x}K_xFe_2As_2$ with x =0.213 (5.6 C/cm^2) and x =0.260 (2.35 C/cm^2) with the degree of orthrhombic distortion, $\delta = (a-b)/(a+b)$, as determined in thermal expansion measurements by Böhmer et al. [18] (open yellow circles) and a product $\rho_t\delta$ (red and magenta lines for 0.213 and 0.260, respectively). Right panel. Comparison of $\Delta\rho(T)$ in the pristine sample of x =0.213 (black line) with a product $\rho_t \times \delta$ (red line) and of the inelastic part of resistivity, $\rho_{t,in} = \rho_t - \rho_{t,0}$, and the orthorhombic order parameter, $\rho_{t,in} \times \delta$ (cyan line).

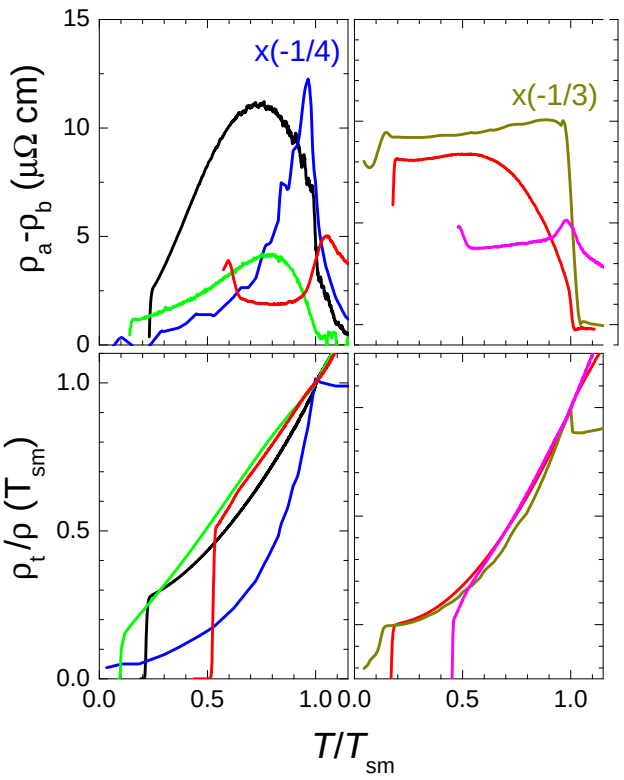


FIG. 8. (Color online) Comparison of the temperature-dependent electrical resistivity anisotropy for clean samples (left top panel) and dirty (top right) samples of various iron based superconductors. The data are presented vs normalized temperature scale, T/T_{C2}. Blue curve is for annealed parent $BaFe_2As_2$ [9], the data are divided by 4, green for FeSe [34], black and red are for $Ba_{1-x}K_xFe_2As_2$ samples x =0.213 and x =0.260, respectively (this study). Yellow curve in the top right panel is for Ru-substituted $BaFe_2As_2$ [11] and is divided by 3. Red line is for the x =0.213 irradiated with 5.6 C/cm^2, magenta line is for x =0.260 sample irradiated with 2.35 C/cm^2. The bottom panels show the temperature dependent resistivities of the same compounds, plotted using normalized $\rho(T)/\rho(T_{C2})$ and T/T_{C2} scales.

radiated sample with x =0.260 (blue line) and $\delta(T)$ for sample with x =0.262. First, we can clearly see that the magnitude of the resistivity anisotropy scales with the degree of the orthorhombic distortion δ, in sharp contrast with the electron-doped side [2]. Second, the product $\delta\rho_t$ gives quite good description of the data for x =0.22 sample (red vs black curve) below approximately 60 K. The difference at higher temperatures is quite notable, however, it is natural that $\Delta\rho(T)$ has a contribution from temperature dependent folding gap opening. In the right panel of Fig. 7 we perform the same analysis for sample x =0.213 in pristine the state. The resistivity anisotropy $\Delta\rho(T)$ (black line) shows close to $T-$linear dependence. The product $\rho_t\delta$ (we use the same $\delta(T)$ as shown in the left panel) captures this $T-$ linear dependence, despite neither $\rho_t(T)$ (black line in Fig. 2) nor $\delta(T)$ showing $T-$linear dependence. The difference with irradiated case is quite notable, since $\Delta\rho(T)$ decreases notably faster than the $\rho_t\delta$ product in the range where the temperature-dependent folding gap opening should have minor effect. The match becomes significantly better if we use only inelastic part of the resistivity, $\rho_{t,in} = \rho_t(T) - \rho_t(0)$, as shown with cyan line.

As a general remark, we should point out, that electron irradiation at the doses used in this study does not introduce variation of carrier density sufficient to have any noticeable impact. This was verified through Hall effect measurements on samples with x =0.20 [21] and is in line with common expectations for metals [37]. So for our discussion we can consider effect only through scattering rate.

The results of this study are in general agreement with the previous studies using annealing to control residual resistivity or the samples with naturally low residual resistivity. For example, the decrease of anisotropy from a large value below T_{C2} on cooling to low temperatures is found in perfectly annealed $BaFe_2As_2$ [9] (blue curve in Fig. 8) and in very clean samples of FeSe [34] (green curve in Fig. 8). We explicitly compare the anisotropy found in these compounds with $Ba_{1-x}K_xFe_2As_2$ samples x =0.213 and x =0.260 in the pristive state. It was argued [9, 11] that the decreasing anisotropy on cooling is determined by contribution of light carriers [38–42], strongly suppressed by disorder scattering. In this respect, close to $T-$ linear dependence of $\Delta\rho(T)$ in the pristine samples with x =0.213 and 0.219 may suggest that this group of carriers suffers critical scattering on approaching $C4$ phase boundary. Indeed fluctuations of nematic order parameter with notable contribution of q =0 component should have notably bigger effect on small pockets of the

Fermi surface.

Strikingly, the increase of residual resistivity with irradiation does not increase anisotropy beyond its maximum value in the clean samples. This fact suggest that $\rho(0)$ does not contribute much to the anisotropy, at least on the hole doped side close to $C_4(x)$ phase boundary.

Interestingly, while $T-$linear dependence is a hallmark of a quantum critical point in the phase diagram of isovalently substituted $BaFe_2(As,P)_2$ [43, 44] and partially electron-doped $Ba(Fe,TM)_2As_2$ [45], the temperature-dependent resistivity in $Ba_{1-x}K_xFe_2As_2$ does not reveal it [16]. Our observation may be suggesting that the reason for this may be phase competition. Indeed, the resistivity in the C_2 phase in the sample with x =0.260 is close to linear, though in a very limited temperature range.

V. CONCLUSIONS

The sign reversal of resistivity anisotropy in the samples of hole-doped $Ba_{1-x}K_xFe_2As_2$ on approaching the reentrant tetragonal phase is insensitive to disorder, opposite to some theory suggestion [8]. The anisotropy at high temperatures does not depend on the residual resistivity, the anisotropy of clean samples with x =0.213 and 0.219 notably decreases on cooling in the pristine samples and stays constant in the samples with high residual resistivity. This study suggests that inelastic scattering responsible for the temperature-dependent part of resistivity is anisotropic, while elastic scattering responsible for residual resistivity is notably less anisotropic. The temperature dependent anisotropy in pristine samples suggests contribution of high mobility carriers subject to scattering on nematic fluctuations.

ACKNOWLEDGMENTS

This research was supported by the U.S. Department of Energy, Office of Basic Energy Sciences, Division of Materials Sciences and Engineering. Ames Laboratory is operated for the U.S. Department of Energy by Iowa State University under Contract No. DE-AC02-07CH11358. Irradiation realized on SIRIUS platform was supported by French National network of accelerators for irradiation and analysis of molecules and materials EMIR&A under project 18-5354.

[1] M. A. Tanatar, E. C. Blomberg, A. Kreyssig, M. G. Kim, N. Ni, A. Thaler, S. L. Bud'ko, P. C. Canfield, A. I. Goldman, I. I. Mazin and R. Prozorov. Phys. Rev. B **81**, 184508 (2010).

[2] J-H. Chu, J. G. Analytis, K. De Greve, P. L. McMahon, Z. Islam, Y. Yamamoto, and I. R. Fisher. Science **329**, 824 (2010).

[3] M. A. Tanatar, A. Kreyssig, S. Nandi, N. Ni, S. L. Bud'ko, P. C. Canfield, A. I. Goldman, and R. Prozorov, Phys. Rev.B **79**, 180508 (R) (2009).

[4] E.C.Blomberg, M.A.Tanatar, R.M.Fernandes, I.I.Mazin, B.Shen, Hai-Hu Wen, M.D. Johannes, J. Schmalian, and R. Prozorov, Nature Comm. **4**, 1914 (2013).

[5] M. P. Allan, T.-M. Chuang, F. Massee, Yang Xie, N. Ni, S. L. Bud'ko, G. S. Boebinger, Q. Wang, D. S. Dessau, P. C. Canfield, M. S. Golden, and J. C. Davis, Nat. Phys. **9**, 220 (2013).

[6] Maria N. Gastiasoro, I. Paul, Y. Wang, P. J. Hirschfeld, Brian M. Andersen, Phys. Rev. Lett. **113**, 127001 (2014).

[7] R. M. Fernandes, E. Abrahams, and J. Schmalian, Phys. Rev. Lett. **107**, 217002 (2011).

[8] M. Breitkreiz, P. M. R. Brydon, and C. Timm, Phys. Rev. B **90**, 121104(R) (2014).

[9] S. Ishida, T. Liang, M. Nakajima, K. Kihou, C. H. Lee, A. Iyo, H. Eisaki, T. Kakeshita, T. Kida, M. Hagiwara, Y. Tomioka, T. Ito, and S. Uchida, Phys. Rev. B **84**, 184514 (2011).

[10] L. Liu, T. Mikami, S. Ishida, K. Koshiishi, K. Okazaki, T. Yoshida, H. Suzuki, M. Horio, L. C. C. Ambolode, II, J. Xu, H. Kumigashira, K. Ono, M. Nakajima, K. Kihou, C. H. Lee, A. Iyo, H. Eisaki, T. Kakeshita, S. Uchida, and A. Fujimori Phys. Rev. B **92**, 094503 (2015).

[11] E. C. Blomberg, M. A. Tanatar, A. Thaler, S. L. Bud'ko, P. C. Canfield, and R. Prozorov, J. Phys. Cond. Matt. **30**, 315601 (2018).

[12] P. C. Canfield and S. L. Bud'ko, Annu. Rev. Condens. Matter Phys. **1**, 27 (2010).

[13] M. A. Tanatar, N. Ni, A. Thaler, S. L. Bud'ko, P. C. Canfield, and R. Prozorov, Phys. Rev. B **82**, 134528 (2010).

[14] X. G. Luo, M. A. Tanatar, J.-Ph. Reid, H. Shakeripour, N. Doiron-Leyraud, N. Ni, S. L. Budko, P. C. Canfield, Huiqian Luo, Zhaosheng Wang, Hai-Hu Wen, R. Prozorov, and Louis Taillefer, Phys. Rev. B **80**, 140503(R) (2009).

[15] E. Hassinger, G. Gredat, F. Valade, S. R. de Cotret, A. Juneau-Fecteau, J.-Ph. Reid, H. Kim, M. A. Tanatar, R. Prozorov, B. Shen, H.-H. Wen, N. Doiron-Leyraud, and Louis Taillefer Phys. Rev. B **86**, 140502(R) (2012).

[16] Y. Liu, M. A. Tanatar, W. E. Straszheim, B. Jensen, K. W. Dennis, R. W. McCallum, V. G. Kogan, R. Prozorov, and T. A. Lograsso, Phys. Rev. B **89**, 134504 (2014).

[17] J. J. Ying, X. F. Wang, T. Wu, Z. J. Xiang, R. H. Liu, Y. J. Yan, A. F. Wang, M. Zhang, G. J. Ye, P. Cheng, J. P. Hu, and X. H. Chen, Phys. Rev. Lett. **107**, 067001 (2011).

[18] A. E. Böhmer, F. Hardy, L. Wang, T. Wolf, P.Schweiss, and C. Meingast, Nat. Comm. **6**, 7911 (2015).

[19] J. M. Allred, S. Avci, D. Y. Chung, H. Claus, D. D. Khalyavin, P. Manuel, K. M. Taddei, M. G. Kanatzidis, S. Rosenkranz, R. Osborn, and O. Chmaissem, Phys. Rev. B **92**, 094515 (2015).

[20] J. M. Allred, K. M. Taddei, D. E. Bugaris, M. J. Krogstad, S. H. Lapidus, D. Y. Chung, H. Claus, M. G. Kanatzidis, D. E. Brown, J. Kang, R. M. Fernandes, I. Eremin, S. Rosenkranz, O. Chmaissem, and

R. Osborn, Nature Phys. **12**, 493 (2016).
[21] Ruslan Prozorov, Marcin Kończykowski, Makariy A. Tanatar, Hai-Hu Wen, Rafael M. Fernandes and Paul C. Canfield, npj Quantum Materials **4**, 34 (2019).
[22] E. I. Timmons, M. A. Tanatar, K. Willa, S. Teknowijoyo, Kyuil Cho, M. Kończykowski, O. Cavani, Yong Liu, T. A. Lograsso, U. Welp, and R. Prozorov, Phys. Rev. B 99, 054518 (2019)
[23] Kyuil Cho, M. Kończykowski, S. Teknowijoyo, M. A. Tanatar, and R. Prozorov, Supercond. Sci. Technol. **31**, 064002 (2018).
[24] M. A. Tanatar, N. Ni, S. L. Bud'ko, P. C. Canfield, and R. Prozorov, Supercond. Sci. Technol. **23**, 054002 (2010).
[25] M. A.Tanatar, R. Prozorov, N. Ni, S. L. Bud'ko, P. C. Canfield, U.S. Patent 8,450,246 (Sept.1, 2011).
[26] E. I. Timmons, M. A. Tanatar, Yong Liu, Kyuil Cho, T. A. Lograsso, M. Kończykowski, and R. Prozorov, Rev. Sci. Instr. **91**, 073904 (2020).
[27] M. A. Tanatar, W. E. Straszheim, Hyunsoo Kim, J. Murphy, N. Spyrison, E. C. Blomberg, K. Cho, J.-Ph. Reid, Bing Shen, Louis Taillefer, Hai-Hu Wen, and R. Prozorov, Phys. Rev. B **89**, 144514 (2014).
[28] E. C. Blomberg, M. A. Tanatar, A. Kreyssig, N. Ni, A. Thaler, Rongwei Hu, S. L. Bud'ko, P. C. Canfield, A. I. Goldman, R. Prozorov. Phys. Rev. B **83**, 134505 (2011).
[29] http://emir.in2p3.fr/ LSI, electron irradiation facility.
[30] https://physics.nist.gov/cgi-bin/Star/estar-u.pl
[31] A.C. Damask and G.J. Dienes, Point Defects in Metals (Gordon & Breach Science Publishers Ltd, London, 1963).
[32] R. Prozorov, M. Kończykowski, M. A. Tanatar, A. Thaler, S. L. Bud'ko, P. C. Canfield, V. Mishra, and P. J. Hirschfeld, Phys. Rev. X **4**, 041032 (2014).
[33] R.M.Fernandes, A.V.Chubukov, J.Schmalian, Nature Phys. **10**, 97 (2014).
[34] M. A. Tanatar, A. E. Böhmer, E. I. Timmons, M. Schütt, G. Drachuck, V. Taufour, K. Kothapalli,A. Kreyssig, S. L. Bud'ko, P. C. Canfield, R. M. Fernandes, and R. Prozorov, Phys. Rev. Lett. **117**, 127001 (2016).
[35] Taichi Terashima, Nobuyuki Kurita, Megumi Tomita, Kunihiro Kihou, Chul-Ho Lee, Yasuhide Tomioka, Toshimitsu Ito, Akira Iyo, Hiroshi Eisaki, Tian Liang, Masamichi Nakajima, Shigeyuki Ishida, Shin-ichi Uchida, Hisatomo Harima, and Shinya Uji, Phys. Rev. Lett. **107**, 176402 (2011).
[36] B. Valenzuela, E. Bascones, and M. J. Calderon, Phys. Rev. Lett. **105**, 207202 (2010).
[37] E. I. Timmons, S. Teknowijoyo, M. Kończykowski, O. Cavani, M. A. Tanatar, Sunil Ghimire, Kyuil Cho, Yongbin Lee, Liqin Ke, Na Hyun Jo, S. L. Bud'ko, P. C. Canfield, Peter P. Orth, Mathias S. Scheurer, and R. Prozorov Phys. Rev. Research **2**, 023140 (2020).
[38] Khuong K. Huynh, Yoichi Tanabe, and Katsumi Tanigaki Phys. Rev. Lett. **106**, 217004 (2011).
[39] Y. Tanabe, K. K. Huynh, T. Urata, S. Heguri, G. Mu, J. T. Xu, R. Nouchi, and K. Tanigaki, Phys. Rev. B **86**, 094510 (2012).
[40] Y. Tanabe, K. K. Huynh, S. Heguri, G. Mu, T. Urata, J. Xu, R. Nouchi, N. Mitoma, and K. Tanigaki, Phys. Rev. B **84**, 100508(R) (2011)
[41] Hsueh-Hui Kuo, Jiun-Haw Chu, Scott C. Riggs, Leo Yu, Peter L. McMahon, Kristiaan De Greve, Yoshihisa Yamamoto, James G. Analytis, and Ian R. Fisher Phys. Rev. B **84**, 054540 (2011).
[42] S. Ishida, T. Liang, M. Nakajima, K. Kihou, C. H. Lee, A. Iyo, H. Eisaki, T. Kakeshita, T. Kida, M. Hagiwara, Y. Tomioka, T. Ito, and S. Uchida, Phys. Rev. B **84**, 184514 (2011).
[43] Y. Nakai, T. Iye, S. Kitagawa, K. Ishida, H. Ikeda, S. Kasahara, H. Shishido, T. Shibauchi, Y. Matsuda, and T. Terashima Phys. Rev. Lett. **105**, 107003 (2010).
[44] M. A. Tanatar, K. Hashimoto, S. Kasahara, T. Shibauchi, Y. Matsuda, and R. Prozorov, Phys. Rev. B **87**, 104506 (2013).
[45] Louis Taillefer, Annu. Rev. Condens. Matter Phys. **1**, 51 (2010).